Orbit determination of space objects based on sparse optical data

A. Milani[1], G. Tommei[1], D. Farnocchia[1], A. Rossi[2], T. Schildknecht[3] and R. Jehn[4]
[1]Dipartimento di Matematica, Università di Pisa, Pisa, Italy
[2]IFAC-CNR, Firenze & ISTI-CNR, Pisa, Italy
[3]Astronomical Institute, University of Bern, Bern, Switzerland
[4]ESA-ESOC, Darmstadt, Germany

Abstract

While building up a catalog of Earth orbiting objects, if the available optical observations are sparse, not deliberate follow ups of specific objects, no orbit determination is possible without previous correlation of observations obtained at different times. This correlation step is the most computationally intensive, and becomes more and more difficult as the number of objects to be discovered increases. In this paper we tested two different algorithms (and the related prototype software) recently developed to solve the correlation problem for objects in geostationary orbit (GEO), including the accurate orbit determination by full least squares solutions with all six orbital elements. Because of the presence in the GEO region of a significant subpopulation of high area to mass objects, strongly affected by non-gravitational perturbations, it was actually necessary to solve also for dynamical parameters describing these effects, that is to fit between 6 and 8 free parameters for each orbit.

The validation was based upon a set of real data, acquired from the ESA Space Debris Telescope (ESASDT) at the Teide observatory (Canary Islands). We proved that it is possible to assemble a set of sparse observations into a set of objects with orbits, starting from a sparse time distribution of observations, which would be compatible with a survey capable of covering the region of interest in the sky just once per night. This could result in a significant reduction of the requirements for a future telescope network, with respect to what would have been required with the previously known algorithm for correlation and orbit determination.

Keywords: orbit determination, space debris

1 Introduction

More than 16,000 objects with diameter larger than approximately 10 cm are orbiting the Earth. Only about 6% of them are operational satellites. All the rest is composed by different types of space debris that now represent a serious hazard to the safe exploitation of the circumterrestrial space.

Most of the catalogued objects reside in the Low Earth Orbit (LEO) regime, i.e. they spend most of their life below 2000 km of altitude. This is the region of space with the highest spatial density of objects and where all the known collisions took place. Nonetheless another region of space hosts a large number of spacecraft that are crucial for our everyday life. It is the geosynchronous region, usually defined as the part of space above about 30000 km of altitude. This paper deals specifically with objects orbiting in this region.

The growing risk posed by the overcrowding of the space calls for a number of measures able in particular to minimize the risk of collision between operational spacecraft and space debris. This requires the accurate knowledge of the orbit of both the objects. Currently the major effort in tracking and cataloguing the space debris population is performed by the United States Strategic Command (USSTRATCOM) using a large network of radar and optical sensors located worldwide. The majority of the larger objects are catalogued by the USSTRATCOM in the Two-Line Element (TLE) catalogue. In this catalogue about 16000 objects are listed along with their current orbital parameters. The limiting size of the objects included in the catalogue (due to limitations in sensors power and in observation and data processing procedures) is about 5 to 10 cm below a few thousands km of altitude and about 0.5 - 1 m in higher orbits up to the geostationary (GEO) ones.

In particular, currently about 1000 objects, with diameter larger than about 1 m, are classified as geosynchronous objects (mean motion between $0.99 \leq$ and 1.01 days and eccentricity not greater than 0.01) in the TLE cataloogue. On the other hand, dedicated optical campaigns from the ESA Space Debris Telescope (ESASDT) (a 1 m telescope located on the Teide vulcano, in the Canary Islands), and from other similar American or Russian sensors, revealed a large number of so-called *uncorrelated objects*, i.e., objects not present in the TLE catalogue. Most of these are probably the result of a still undetermined number of explosions occurred to spacecraft and upper stages. Dedicated optical observation campaigns were performed to characterize the environment in this orbital region (e.g., [13]) for objects down to a few tens of cm.

Moreover, in recent years, a peculiar population of objects having mean motion around 1 and high eccentricity (as high as 0.55) was detected by the ESASDT ([12]). It was shown that these are objects with very high area to mass ratio (ranging between 1 m^2/kg up to 30 m^2/kg) whose dynamics is therefore strongly perturbed by the solar radiation pressure that significantly affects their eccentricity (and also their inclination) with small effects on the total energy of the orbit and, therefore, on the semi-major axis or mean motion ([4]). Most probably these objects are remnants of thermal blankets or multi-layer insulation (MLI) either detached from aging spacecraft or ejected by explosive fragmentations of old spacecraft. It is worth noting that, from an observational point of view, these objects represent a particularly demanding task. Their dynamics is extremely difficult to model, due to the large influence of the solar radiation pressure, further complicated by the unknown and rapidly changing physical properties of the objects. This translates in a comparable difficulty in the determination of their orbits. In Sec. 3 the algorithm used for the orbit determination of high area-to-mass ratio (A/M) objects will be described.

Until recently, most of the dedicated observations have not been devoted to cataloguing purposes and have not led to a full orbit determination. The information obtained in the surveys made since 1999 are mainly statistical since no attempt has been made to catalog the objects. This means that some objects may have been observed multiple times. From a probabilistic analysis, in ([3]) it is pointed out that the population of debris, brighter than visual magnitude 18.5, inferred from the ESASDT, may indeed suffer from multiple observations. This might have lead to the over-estimation of this particular population by a factor of about 5.

The procedures described in this paper were devised to solve this problem and to provide effective algorithms for the building of a European catalogue, analogous to the TLE one, foreseen in the framework of the European Space Situation Awareness (SSA) initiative. The SSA intends to provide Europe with an autonomous capacity to monitor

the circumterrestrial space allowing a safe exploitation of this resource.

In Sec. 2 and Sec. 3 we briefly recall the main features of the algorithms developed by our group in the last years for the orbit determination of space objects. Then the dataset used to validate the algorithms is presented. And, finally, the results obtained are presented and discussed.

2 Algorithms

Given two or more sets of observations, the main problem is how to identify which separate sets of data belong to the same physical object (the so-called *correlation* problem). Thus the orbit determination problem needs to be solved in two stages: first different sets of observations need to be correlated, then an orbit can be determined; this combined procedure is called *linkage* in the literature (see [6]).

Two different linkage methods were developed in the last few years. The algorithms are fully described in ([15]), ([2]), ([11]), ([1]). In this section, for ease of reading, we will briefly recall the main features of these algorithms, directing the reader to the above cited papers for the full mathematical treatment.

2.1 Observations and attributables

To understand the results presented in the following sections some nomenclature and definitions have to be introduced.

The batches of observations which can be immediately assigned to a single object give us a set of data that can be summarized in an *attributable*, that is a 4-dimensional vector. To compute a full orbit, formed by 6 parameters, we need to know 2 further quantities.

Let $(\rho, \alpha, \delta) \in \mathbb{R}^+ \times [0, 2\pi) \times (-\pi/2, \pi/2)$ be topocentric spherical coordinates for the position of an Earth satellite. The angular coordinates (α, δ) are defined by a topocentric reference system that can be arbitrarily selected. Usually, in the applications, α is the right ascension and δ the declination with respect to an equatorial reference system (e.g., J2000). The values of range ρ and range rate $\dot{\rho}$ are not measured.

We shall call *optical attributable* a vector

$$\mathcal{A}_{opt} = (\alpha, \delta, \dot{\alpha}, \dot{\delta}) \in [0, 2\pi) \times (\pi/2, \pi/2) \times \mathbb{R}^2 \,,$$

representing the angular position and velocity of the body at a time t in the selected reference frame (for the definition of the radar-attributable see [15]).

Given the attributable $\mathcal{A}$, to define an orbit the values of two unknowns quantities (e.g., ρ and $\dot{\rho}$) need to be found at the same instance in time as the attributable. These two quantities, together with $\mathcal{A}$, give us a set of *attributable orbital elements*

$$X = [\alpha, \delta, \dot{\alpha}, \dot{\delta}, \rho, \dot{\rho}]$$

at a time $\bar{t}$, computed from t taking into account the light-time correction: $\bar{t} = t - \rho/c$ (c being the velocity of light). Of course the information on the observer station must be available.

Starting from an attributable, we would like to extract sufficient information in order to compute full preliminary orbits.

2.2 Virtual debris algorithm

The first algorithm developed is called the Virtual debris algorithm and makes use of the so-called *admissible region*.

The admissible region replaces the conventional confidence region as defined in the classical orbit determination procedure. The main requirement is that the geocentric energy of the object is negative, so that the object is a satellite of the Earth.

Given the geocentric position $\mathbf{r}$ of the debris, the geocentric position $\mathbf{q}$ of the observer, and the topocentric position $\boldsymbol{\rho}$ of the debris we have $\mathbf{r} = \boldsymbol{\rho} + \mathbf{q}$. The energy (per unit of mass) is given by

$$\mathcal{E}(\rho, \dot{\rho}) = \frac{1}{2}||\dot{\mathbf{r}}(\rho, \dot{\rho})||^2 - \frac{\mu}{||\mathbf{r}(\rho)||}\,, \tag{1}$$

where μ is the Earth's gravitational parameter. Then a definition of admissible region such that only satellites of the Earth are allowed includes the condition

$$\mathcal{E}(\rho, \dot{\rho}) \leq 0. \tag{2}$$

This condition translates in a region of $(\rho, \dot{\rho})$ having at most two connected components (even if in a large number of numerical experiments with objects in Earth orbit, we have not found examples with two connected components.) The admissible region needs to be compact in order to have the possibility to sample it with a finite number of points, thus a condition defining an inner boundary needs to be added. The choice for the inner boundary depends upon the specific orbit determination task: a simple method is to add constraints $\rho_{min} \leq \rho \leq \rho_{max}$ allowing, e.g., to focus the search of identifications to one of the three classes LEO, MEO (Medium Earth Orbits) and GEO. Another natural choice for the inner boundary is to take $\rho \geq h_{atm}$ where h_{atm} is the thickness of a portion of the Earth atmosphere in which a satellite cannot remain in orbit for a significant time span. As an alternative, it is possible to constrain the semimajor axis to be larger than $R_\oplus + h_{atm} = r_{min}$, where h_{atm} is the radius of the Earth atmosphere. The qualitative structure of the admissible region is shown in Fig. 1. The shaded region of Fig. 1 can be further constrained and reduced excluding trajectories impacting the Earth in less than one revolution, which means to impose that the perigee is larger than a given value r_{min} (see [1]).

Once the admissible region is defined it has to be discretized sampling it to generate a swarm of *virtual debris*. This is done using the Delaunay triangulation ([8]). The idea is to generate a swarm of virtual debris X_i, corresponding to the nodes of the admissible region of one of the two attributables, let us say $\mathcal{A}_1$. Then we compute, from each of the X_i, a prediction $\mathcal{A}_i$ for the epoch t_2, each with its covariance matrix $\Gamma_{\mathcal{A}_i}$. Thus for each virtual debris X_i we can compute an attribution penalty K_4^i ([9], [11][Cap. 8]) and use the values as a criterion to select some of the virtual debris to proceed to the orbit computation.

Thus the procedure is as follows: we select some maximum value K_{max} for the attribution penalty and if there are some nodes such that $K_4^i \leq K_{max}$ we proceed to the correlation confirmation. If this is not the case, we can try with another method, such as the one described in Sec. 2.3.

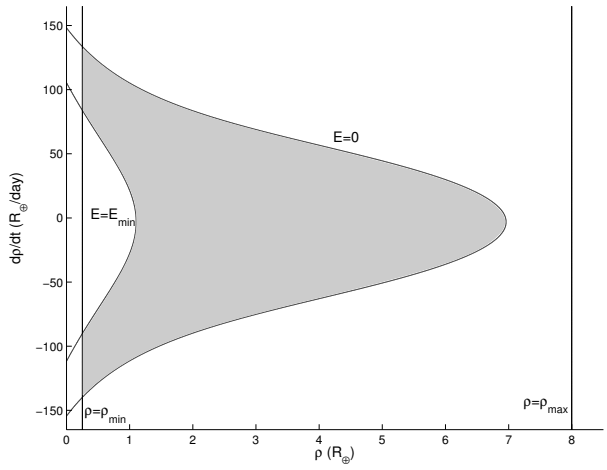

Figure 1: An example of admissible region, optical case, in the $(\rho, \dot{\rho})$ plane. The region (painted in grey) is bounded by two level curves of the energy, $(E = E_{min})$ and $(E = 0)$, and by the two conditions on the topocentric distance $(\rho = \rho_{min}$ and $\rho = \rho_{max})$.

2.3 Keplerian integrals method

An alternative method to produce preliminary orbits starting from two attributables $\mathcal{A}_1$, $\mathcal{A}_2$ of the same object at two epoch times t_1 and t_2, was proposed for the asteroid case in [2] and is based on the two-body integrals. The method was implemented and adapted to the space debris case ([1]). Once more the procedure is applicable to both optical and radar observations, but only the optical case will be recalled here. We assume that the orbit between t_1 and t_2 is well approximated by a Keplerian 2-body orbit, with constant energy $\mathcal{E}$ and angular momentum vector $\mathbf{c}$:

$$\begin{cases} \mathcal{E}(t_1) - \mathcal{E}(t_2) = 0 \\ \mathbf{c}(t_1) - \mathbf{c}(t_2) = 0 \end{cases} . \tag{3}$$

Solving the system (3) requires a complex analytical and numerical procedure, involving algebraic equations. This is detailed in [2] and [1] and it is not worth recalling here. Once the roots of the equation are obtained, given all the roots which could be real, we select the positive couples (ρ_1, ρ_2) and remove the spurious ones. If the number of remaining solutions is zero, the attributables cannot be correlated with this method, otherwise the selected couple represents the sought for solution.

Once a solution of (3) is computed the values of attributable elements can be obtained for the epochs $\bar{t}_1$ and $\bar{t}_2$, and they can be converted into the usual Keplerian elements:

$$(a_j, e_j, I_j, \Omega_j, \omega_j, \ell_j) \ , \ j = 1, 2 \ ,$$

where ℓ_j are the mean anomalies. The first four Keplerian elements $(a_j, e_j, I_j, \Omega_j)$ are functions of the 2-body energy and angular momentum vectors $\mathcal{E}_j$, $\mathbf{c}_j$, and are the same for $j = 1, 2$. Thus the result can be assembled in the 8-dimensional vector:

$$H = (V, \Phi_1, \Phi_2) \quad , \quad V = (a, e, I, \Omega)$$

$$\Phi_1 = (\omega_1, \ell_1) \ , \ \Phi_2 = (\omega_2, \ell_2) \tag{4}$$

There are compatibility conditions between Φ_1 and Φ_2 to be satisfied if the two attributables belong to the same object:

$$\omega_1 = \omega_2 \ , \ \ell_1 = \ell_2 + n(\bar{t}_1 - \bar{t}_2) \ , \tag{5}$$

where $n = n(a)$ is the mean motion. We cannot demand the exact equality in the formulae above, because of various error sources, including the uncertainty of the attributable, and the changes on the Keplerian integrals due to the perturbations with respect to the 2-body model. Thus we need a metric to measure in an objective way the residuals in the compatibility conditions. The two attributables $\mathcal{A}_1, \mathcal{A}_2$ have been computed from the observations by using a least squares fit to the individual observations, thus 4×4 covariance matrices $\Gamma_{\mathcal{A}_1}$ and $\Gamma_{\mathcal{A}_2}$ are available; they can be used to form the block diagonal 8×8 covariance matrix for both attributables $\Gamma_{\mathcal{A}}$. The Keplerian integral method allows to compute explicitly the vector H of (4) and, by means of the implicit function theorem, its partial derivatives, thus it is possible by the standard covariance propagation formula [11][Sec. 5.5] to compute also Γ_H, the covariance of H. With another transformation we can compute the average elements $\Phi_0 = (\Phi_1 + \Phi_2)/2$ (as the best value for the angular elements at time $\bar{t}_0 = (\bar{t}_1 + \bar{t}_2)/2$) and the discrepancy $\Delta\Phi$ in the compatibility conditions (5), and to propagate the covariance also to this 8-dimensional vector:

$$\Gamma_{\mathcal{A}} \Longrightarrow \Gamma_H \Longrightarrow \Gamma_{V,\Phi_0,\Delta\Phi} \ .$$

The above argument is a generalization of the one in [2], where explicit computations are given for the optical attributables case.

In the 8×8 covariance matrix $\Gamma_{V,\Phi_0,\Delta\Phi}$, the lower right 2×2 block is the marginal covariance matrix of $\Delta\Phi$, from which we can compute the normal matrix and the χ^2:

$$C_{\Delta\Phi} = \Gamma_{\Delta\Phi}^{-1} \quad , \quad \chi^2_{\Delta\Phi} = \Delta\Phi \cdot C_{\Delta\Phi} \, \Delta\Phi \ ,$$

which can be used as control, that is the discrepancy in the compatibility conditions is consistent with the observation error and the correlation between the two attributables is considered possible only if $\chi^2_{\Delta\Phi} \leq \chi^2_{max}$.

The upper left 6×6 block is the covariance matrix of the preliminary orbit, that is of the orbital elements set (V, Φ_0) (at epoch $\bar{t}_0$). Although this preliminary orbit is just a 2-body solution, it has an uncertainty estimate, arising from the (supposedly known) statistical properties of the observational errors. This estimate neglects the influence of perturbations, such as the spherical harmonics of the Earth gravity field, the lunisolar differential attraction and the non-gravitational perturbations; nevertheless, if the time span $\bar{t}_2 - \bar{t}_1$ is short, the covariance obtained above can be a useful approximation. Recently the method was generalized, including the effect due to the non-spherical shape of the Earth ([1]), thus allowing its application also to objects in LEO. On the other hand since the present paper deals only with high Earth orbit data, where the effect of J_2 on the angular momentum of the objects is strongly reduced by the distance from the center of the Earth, all the analysis presented in this paper was performed without the inclusion of the J_2 effect.

Note that there are some cases in which the Keplerian integrals method can not be applied. We have to avoid the condition $(\mathbf{q}_1 \times \hat{\boldsymbol{\rho}}_1) \times (\mathbf{q}_2 \times \hat{\boldsymbol{\rho}}_2) = 0$, where $\mathbf{q}_1$ and $\mathbf{q}_2$ are the observer geocentric positions at the instants t_1 and t_2. This can happen when:

- $\mathbf{q}_1$ is parallel to $\hat{\boldsymbol{\rho}}_1$, i.e., the observation at time t_1 is done at the observer zenith;
- $\mathbf{q}_2$ is parallel to $\hat{\boldsymbol{\rho}}_2$, i.e., the observation at time t_2 is done at the observer zenith;
- $\mathbf{q}_1$, $\mathbf{q}_2$, $\hat{\boldsymbol{\rho}}_1$ and $\hat{\boldsymbol{\rho}}_2$ are coplanar. This case arises whenever a geostationary object is observed from the same station at the same hour of distinct nights.

As it is normal, the mathematical singularity is surrounded by a neighborhood in which the method is possible for zero error (both zero observational error and zero rounding off in the computation), but is not applicable in practice due to the limited numerical accuracy; e.g., this method fails even for non-geostationary, nearly geosynchronous orbits with hours of observations over different nights differing by only a few minutes each night. Note that in an observing strategy optimized for the use of this method, this occurrence can be easily avoided.

2.4 Correlation confirmation

The multiple orbits obtained from the solutions of the algebraic problem are just preliminary orbits, solution of a 2-body approximation (as in the classical methods of Laplace and Gauss). They have to be replaced by least squares orbits, with a dynamical model including all the relevant perturbations.

Even after confirmation by least squares fit, it might still be the case that some linkages with just two attributables can be *false*, that is the two attributables might belong to different objects. This is confirmed by the tests with real data reported in [16] for the virtual debris method and in [10] for the Keplerian integrals method. Thus every linkage of two attributables needs to be confirmed by correlating a third attributable.

The process of looking for a third attributable which can also be correlated to the other two is called *attribution* ([6, 7]). From the available 2-attributable orbit with covariance we predict the attributable $\mathcal{A}_P$ at the time t_3 of the third attributable, and compare with $\mathcal{A}_3$ computed from the third set of observations. Both $\mathcal{A}_P$ and $\mathcal{A}_3$ come with a covariance matrix, we can compute the χ^2 of the difference and use it as a test. For the attributions passing this test we proceed to the differential corrections. The procedure is recursive, that is we can use the 3-attributable orbit to search for attribution of a fourth attributable, and so on. This generates a very large number of many-attributable orbits, but there are many duplications, corresponding to adding them in a different order.

A specific procedure, called *correlation management* is used to remove duplicates (e.g., $A = B = C$ and $A = C = B$) and inferior correlations (e.g., $A = B = C$ is superior to both $A = B$ and to $C = D$, thus both are removed). The output catalog after this process is called normalized. In the process, we may try to merge two correlations with some attributables in common, by computing a common orbit ([9]).

Due to the characteristics of the two methods briefly outlined in this Section, it can be noticed that the two algorithms have different ranges of application. The virtual debris algorithm should be applied to short time intervals between observed arcs, less than one orbital period or at most a few orbital periods. The Keplerian integrals method, thanks to the constancy of the integrals of the 2-body problem even over significant time intervals, can be used for longer time spans, spanning several orbital periods. On the other hand, it is near to a singularity for very short time spans and in some other near-resonance conditions, such as observations of a geosynchronous orbits at the same hour in different

nights. We conclude that each method should be used in the cases in which it is most suitable as will be illustrated in Sec. 5.

3 Non gravitational perturbation model

The solar radiation pressure represents the largest non-gravitational perturbation acting on a spacecraft in high Earth orbit. As detailed in ([5]), the solar radiation pressure mainly accounts for periodic perturbations in the eccentricity e and inclination i of the orbit. On the other hand, whenever the orbit is such that the satellite periodically enters the shadow of the Earth (as in the case of the GEO satellites), the eclipses have an important perturbative effect on the orbit, because there could be a secular effect on semimajor axis a, thus an accumulated along track displacement quadratic in time. The situation becomes worse in the case of the high A/M objects where the solar radiation pressure can become the dominant perturbative term beyond the spherical Earth approximation for $A/M \simeq 10$ m^2/kg. Therefore the perturbations can result in significant changes in a and/or in very large values of e and i ([17]). Moreover for this kind of objects very little is known about their physical properties thus preventing an effective modelling of the non-gravitational perturbations affecting them.

Other non-gravitational effects can contribute with a secular perturbation in a, see e.g. [11, Chap. 14], including the so-called Yarkovsky effect, which is the result of a systematic anisotropic emission of radiation due to uneven external surface temperature, and indirect radiation pressure, due to radiation reflected and/or re-emitted by the Earth. These effects are smaller than the main component of radiation pressure in terms of the instantaneous value of the force, by a factor typically somewhere between a few parts in 1000 and a few parts in 100. Still, they can be the dominant source of perturbation in the satellite position after a number of orbital periods, while the main source of short term perturbations remains, in almost all cases, the main anti-Sun component.

For the above reasons an adaptive non-gravitational perturbations semi-empirical model, with the following properties was developed:

- For observed arcs either of total duration ≤ 0.01 days, or with less than 3 tracklets, we use no non-gravitational perturbation model, thus we solve for each set of correlated observations for only 6 orbital elements.
- For observed arcs with at least 3 tracklets and total duration > 0.01 days we use a model with direct radiation pressure, only the anti-Sun component, and with a free A/M parameter[1], thus we solve for at least 7 parameters.
- For observed arcs with at least 4 tracklets and total duration > 2 days we use a model with an additional secular along track term giving quadratically accumulated along track displacement, with a free multiplicative parameter with the dimension of A/M (to ease comparison with the other term) thus we solve for 8 parameters.

The direct radiation pressure model includes a model for eclipses (with penumbra), thus it already includes some quadratic perturbations when the orbit is subject to eclipses.

The controls used to activate the more complex models take into account not just the time span but also the amount of observational data available in order to preserve

[1]Actually, the parameter incorporates the so-called *reflection coefficient*, which cannot be separately determined and is anyway close to 1.

the over-determined nature of the least square fit. E.g., if we were to use 2 tracklets in an 8-parameters fit, there would be only 8 equations in 8 unknown. In particular, the Keplerian Integrals method of Section 2.3 has shown a good capability of finding an approximating 2-body solution even for cases in which the orbit is moderately perturbed, such as a large A/M case over several days. If we were to attempt a fit with non-gravitational perturbations with the initial correlation, that is still with 2 tracklets, a 7-parameter orbit would be very weakly determined and instabilities of the differential corrections iterations could result in abandoning many good correlations.

Note that the semi-empirical models, such as this one, contain terms which are not in a one to one correspondence with physical effects. E.g., the along track term may represent a Yarkovsky effect as well as resulting in secular perturbations in a.

Although the parameters are fitted, one caution is important: when using a semi-empirical parameter such as A/M, we need to constrain the values which can be determined within a physically meaningful range. We are currently using $[-1, +200]$ as the control range for the A/M coefficient (in m^2/kg) for direct radiation pressure, and $[-1, +2]$ for the one of the along track force.

4 Observations and survey strategies

For the purpose of this study it was decided to use existing data from observations performed at ESA's 1-meter Space Debris Telescope (ESASDT). The data stems from surveys and so-called follow-up observations of the year 2007. The former were optimized to search for small-size debris in the GEO region and the geostationary transfer orbit region (GTO), with the main objective to derive statistical information. Follow-up observations, on the other hand, are used to maintain a catalogue of debris objects to allow for detailed analysis of physical characteristics, e.g. by acquiring multi-color photometry, spectra, etc. It is important to notice that the surveys were not designed in a way to serve as a test for a "survey only" catalogue build-up and maintenance strategy. As a consequence the resulting observations were not intended to serve as test data for orbit determination or tracklet correlation algorithms. Survey strategies optimized to build-up and maintain a catalogue of objects without the need of explicit follow-up observations are feasible, but should obviously be designed in close connection with the tracklet correlation and orbit determination algorithms.

Space debris observations at the ESASDT are organized as monthly observation campaigns consisting of about 10 to 14 nights centered on New Moon. Generally, there are three types of observations performed:

- *GEO surveys*, with a search area optimized for GEO orbits with $0 - 20^\circ$ inclination. The tracking during the exposure (so-called 'blind tracking') is optimized for object in GEO.

- *GTO surveys*, with a search area optimized for GTO orbits with $0 - 20^\circ$ inclination (Ariane GTO launches). The blind tracking during the exposure is optimized for objects in GTO.

- *Follow-up observation* for a subset of the objects discovered in surveys (maintenance of a catalogue of debris objects). The total arcs covered by follow-up observations range from a few hours up to many months.

Table 1: ESA GEO and GTO Campaigns

	Jan - Dec 2007 GEO/GTO
Frames	56000
Scanned Area	7600 deg^2
Total Observation Time	81 nights / 461 h
GTO / Follow-up	180 h/193 h
Correlated tracklets	483
Correlated objects	241
Uncorrelated tracklets	618

Table 1 gives an overview of all the ESA GEO and GTO campaigns from January 2007 until December 2007. The terms "correlated" and "uncorrelated" refer to objects/tracklets for which a corresponding catalogue object could or could not be identified, respectively. The identification procedure, or "correlation procedure", is based on comparing the observed orbital elements and the observed position in longitude and latitude of the object at the observation epoch with the corresponding data from the catalogue. We used the unclassified part of the USSTRATCOM catalogue as our reference.

The data set for the test of the algorithms was provided by the Astronomical Institute of the University of Bern (AIUB). It contained the tracklets of all correlated and uncorrelated "objects" from the 2007 GEO and GTO surveys, as well, as the tracklets from all follow-up observations. For this data independent information about tracklets belonging to one and the same object, at least for the correlated objects and the objects which were followed-up intentionally, are available.

The data set contains 3177 tracklets, among them

- 977 uncorrelated tracklets,
- 747 correlated tracklets of 349 correlated objects ("correlated" = correlated with USSTRATCOM TLE catalogue),
- 1453 tracklets from intentional follow-up observations of 240 objects.

The uncorrelated and the correlated tracklets were found in the GEO and GTO surveys, but also during follow-up observations instead or in addition to tracklets of objects to be followed up. The surveys covered the GEO region rather homogeneously but were not optimized to re-observe objects, e.g. from night to night. Based on results by [3] and [14] these 977 uncorrelated tracklets could belong to $300 - 500$ objects.

The tracklets of the objects which were intentionally followed-up have very particular characteristics, which are non-typical for survey observations and thus worth mentioning. These objects belong to an AIUB-internal catalogue of small-size debris in GEO- or GTO-like orbits. The catalogue is biased towards objects with high area-to-mass ratio due to deliberate selection. For a newly detected object the standard procedure consists of acquiring 1-4 follow-up observations during the night of discovery, resulting in arcs of 0.5-5 hours. Additional 1-2 follow-up observations are then performed during the nights following the discovery, eventually followed by regular observations every month. It is,

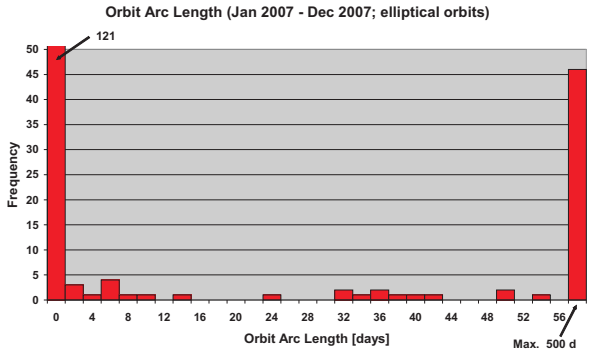

Figure 2: Histogram of the arc length for the objects which were intentionally followed-up during the 2007 campaigns.

again, worth noticing that the temporal distribution of these follow-up observations does not at all represent typical space debris survey or surveillance (SSA) scenarios.

The available arc length for the majority of the objects which were followed-up during the 2007 campaigns is less than one day (see Fig. 2). For 46 objects, however, an arc length of more than 57 days is available.

The tracklet data was provided in the form of so-called **"tracklet files"** of the Pan-STARRS Data Exchange Format (DES). The DES is described by a complex document, which introduces the necessary concepts, fixes one standard terminology, defines the data types with an object-oriented style, assigns formats and procedures for exporting/importing all the data types.

In these files, observations pertaining to the same tracklet are identified by a unique "tracklet identifier". The assignment of individual observations to a tracklet is (by definition) done by the "observer" as it is intimately related with the survey and the object detection algorithms. A typical survey will, though, not provide any information about "objects", i.e. about the mutual correlation of tracklets. However, if such information is available, it may be coded in the so-called "secret names". This information (discriminating between uncorrelated tracklets, correlated objects or follow-up observation of correlated objects) is not to be used in the test phase, but it is stored in order to allow a final comparison with the "ground truth".

5 Results from a one year experiment

The new algorithms and the related software described in Sec. 2 were applied to the data set described in the previous section. The purpose was to show that they are adequate for a future catalog buildup activity by ESA, e.g., in the context of the SSA initiative. Thus we selected a time interval long enough that we can presume a future SSA survey would have observed all target objects within such a period, and short enough to allow for accurate orbit determinations with our semi-empirical non-gravitational perturbations model. We selected the lunation as a kind of natural time unit for observations. The tracklets of objects observed several times within one lunation should be correlated. On the contrary, objects observed only once per lunation may not be correlated, because this

is well beyond the SSA specifications.

5.1 The test on one year of data

As explained in Sec. 4 the data set contained three classes of tracklets: the ones correlated by attribution to TLE objects, the ones correlated by AIUB (in most cases, by targeted follow up), and the ones for which no correlation was previously known.

The database of tracklets was split in 12 lunations. The algorithms described in Sec. 2 were applied to each lunation separately. The correlations within each lunation are normalized, thus there are no duplicates, using the correlation management procedure (see Sec. 2.4).

Out of 3177 input tracklets, 1503 were correlated, 1674 left uncorrelated. Of course we have no way to know how many should have been correlated, that is how many physically distinct objects are there: in particular, objects re-observed at intervals longer than 10 days have escaped correlation, because we did not try to perform the first step when the time span between two tracklets exceeds 10 days. As already pointed out in Sec. 4, the observations were not scheduled to allow for orbit determination of all the objects, but only for some of them, in particular the uncorrelated objects, which were of interest as candidate high A/M cases.

5.2 The global orbit catalog

Joining the orbits computed in each lunation, we obtained 202 correlations with a good orbit and more than two tracklets. This process might generate duplications of orbits for the same object. In fact if two orbits for the same object are computed in different lunations it is not always possible to correlate them, especially if the two lunations are not consecutive. We plan to investigate the issue of duplications in this catalogue in the future.

Figures 3–6 show the distribution of the computed orbits in terms of orbital elements and absolute magnitude.

The orbits in the (a, e) plane (Fig. 3) show a concentration of objects with semimajor-axis close the geostationary radius, including some with high eccentricity. Some of these latter objects have a high value of the A/M parameter, as described in Sec. 1. In the upper left corner the objects in GTO can be found with $e \simeq 0.7$. Fig. 4 shows the same orbits in the (I, e) plane.

Fig. 4 shows an apparent lack of really geostationary orbits, with low e and I: actually there is only one orbit with $e < 0.01$ and $I < 5°$. This is due to the fact that the survey conducted by the ESASDT in 2007 had the purpose of discovering new objects, and the geostationary objects are mostly active satellites, whose orbits and ephemerides are known. Thus the fields of view were on purpose avoiding the geostationary line of Fig. 3.

Figs. 5 and 6 show the distribution of eccentricity/inclination versus intrinsic luminosity of the objects, the latter described in the absolute magnitude scale. Unfortunately it is not easy to convert an absolute magnitude into a size, because of the wide range of albedo values and also because of irregular shapes. However, if we could assume albedo 0.1 and a spherical shape, we would get a diameter ranging between 10 m and $\simeq$ 30 cm for the correlated objects. Thus the largest objects should be satellites (at low e) and rocket stages (near GTO), the smallest are certainly debris.

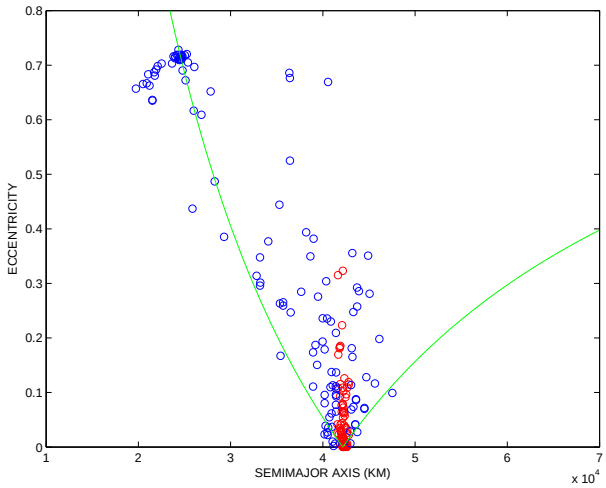

Figure 3: Distribution in semimajor-axis vs. eccentricity of the computed orbits. Red circles indicate objects with semimajor-axis between 41464 and 42864 km, i.e. nearly geostationary. Blue circles indicate all the other orbits. The green lines bound orbits crossing the GEO radius at apogee (left curve) or at perigee (right curve).

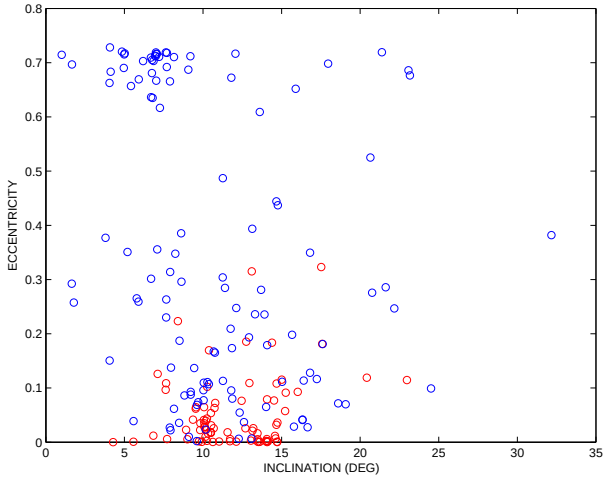

Figure 4: Distribution in inclination vs. eccentricity of the computed orbits. Red circles indicate objects with semimajor-axis between 41464 and 42864 km, i.e. nearly geostationary. Blue circles indicate all the other orbits.

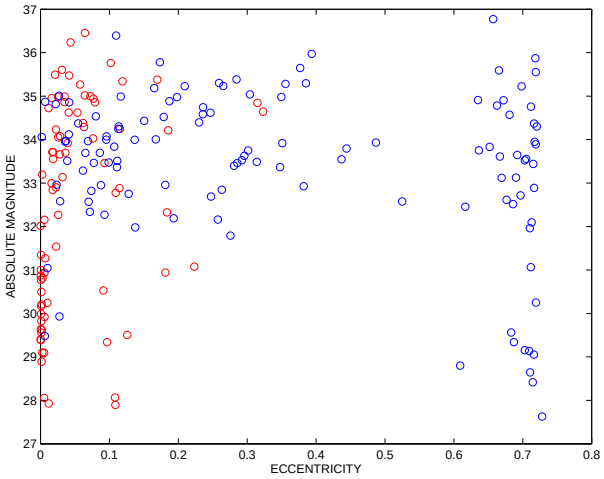

Figure 5: Distribution in eccentricity vs. absolute magnitude of the computed orbits. Red circles indicate objects with semimajor-axis between 41464 and 42864 km, i.e. nearly geostationary. Blue circles indicate all the other orbits.

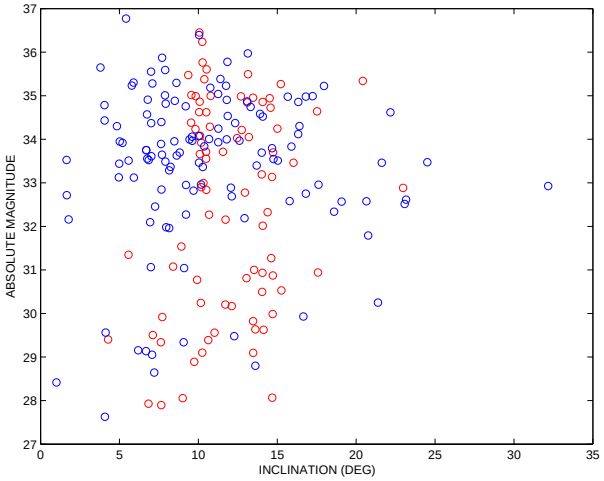

Figure 6: Distribution in inclination vs. absolute magnitude of the computed orbits. Red circles indicate objects with semimajor-axis between 41464 and 42864 km, i.e. nearly geostationary. Blue circles indicate all the other orbits.

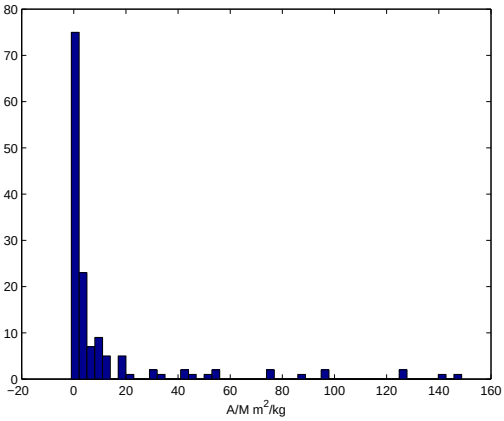

Figure 7: Histograms showing the number of objects with a significant value for A/M parameter.

The existence of objects with high e and also I was already well known, what is interesting is that some of these have a quite large cross section. To understand the dynamics of such objects is a challenge, which requires advanced models and a good data set of both astrometry and photometry.

5.3 Determination of non-gravitational parameters

As previously pointed out in Sec. 3 it is important to succeed in determining the perturbations due to non-gravitational effects. As described in Sec. 2, the algorithms were modified in order to handle this task. This implies not just to have a non-gravitational perturbation model in the orbit propagator, but to apply the adaptive model progressively as the correlations build up, with the semi-empirical parameters gradually added to the list of variables to be solved.

In the Figs. 7 and 8 the distribution of the values of non-gravitational parameters computed for a subsample of the objects displayed in Fig. 3 are shown. In particular, the A/M parameter was computed for 143 objects and for 59 objects also the along track perturbation (called Yark parameter) was determined. Note that the name of the latter parameter is just suggestive, we cannot discriminate between a true Yarkovsky effect (due to thermal emission) from an effect of direct radiation pressure on a complex shape debris, as discussed in Sec. 3.

Whereas the bulk of the objects lies in the first histogram bin, a significant fraction of them belong to the so-called large area to mass ratio population. Note that a few objects display a huge value of A/M (> 100 m^2/kg) and Yark (absolute value > 0.5 m^2/kg). However, these cases typically have a large uncertainty, possibly due to the too short time span between the correlated tracklets.

The problem is that we did not have any "ground truth" to compare our results on non-gravitational perturbations; for this we would need to have a catalog with orbits and non-gravitational parameters from other sources. On the other hand the objects on which to perform such a comparison should be carefully selected, among those with the best determination not just of the orbit but also of the semi-empirical parameters. These

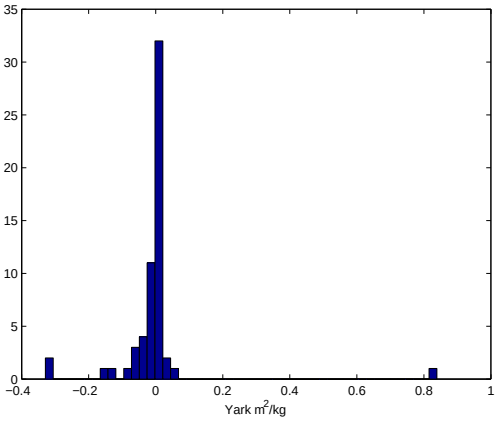

Figure 8: Histograms showing the number of objects with a significant value for the along track perturbation Yark parameter.

"good cases" might require fitting more than one month of data. This problem will also need to be further investigated.

5.4 Assessment of the results

Once a catalog of orbit is obtained it would be important to be able to judge the performance of the algorithms and the reliability of the catalogue itself. In the present analysis no absolute "ground truth" (that is an orbit catalog used as input for the data simulation) was available to validate the catalog. Nonetheless a meningful comparison, giving an indication of the validity of the procedure, was possible by comparing with the correlation results obtained by the group that produced the data set itself. This implies that it is not always possible, in case of a discrepancy between the two catalogs, to decide "who is right". Fortunately, this was not necessary. The goal was to show that the new algorithms allow to obtain substantially the same results obtained by the AIUB group, without having access to the scheduling information. Namely, if an uncorrelated object has been the target of deliberate follow up, the AIUB group had the correlation information a priori (and the same information could be obtained for a correlated object, just by comparing with the ephemerides). On the other hand the present analysis did not use any a priori information.

To make an in depth study, we selected the two lunations which included the largest number of tracklets, namely the first and the second one. In Tables 2 and 3 we show a summary of the results obtained.

The meaning of the table columns is the following:

- *equal* indicates the cases in which the new algorithms obtained the same correlation reported by AIUB;
- *larger* indicates the cases in which the new algorithms added some additional tracklets (marked NS) to those considered by AIUB in their correlation;

Table 2: Summary of the comparison with AIUB for the first lunation. Between parenthesis we highlight the number of occurrences where we identified the reason for the smaller or missed correlations with an observation strategy not optimized for our algorithms. See text for details.

Number of Tracklets	Equal	Larger	New	Smaller	Missed	Mixed
16	-	-	-	-	-	1
10-11	1	-	-	1	-	-
7-8	7	1	1	-	-	-
4-6	7	3	-	1	1 (1)	-
3	4	3	2	3 (3)	1 (1)	-

Table 3: Summary of the comparison with AIUB for the second lunation. Between parenthesis we highlight the number of occurrences where we identified the reason for the smaller or missed correlations with an observation strategy not optimized for our algorithms. See text for details.

Number of Tracklets	Equal	Larger	New	Smaller	Missed	Mixed
11-12	-	3	-	-	-	1
7-9	3	-	-	3 (1)	-	1
4-6	12	5	-	8 (4)	7 (6)	-
3	10	1	3	3 (2)	6 (4)	1

- *new* indicates correlations not found by AIUB, i.e., orbits computed by the new algorithms using just NS tracklets;
- *smaller* indicates the cases in which the new algorithms got a correlation using a subset of the tracklets used by AIUB;
- *missed* indicates the cases in which the new algorithms did not get the correlation reported by AIUB;
- *mixed* indicates the cases in which the new algorithms obtained a correlation using a partly different set of tracklets with respect to AIUB. That is the new algorithms got a correlation using some (but not all) of the tracklets exploited by AIUB and, at the same time, added some NS tracklets.

A deeper analysis of the underlying reasons for the smaller and missed correlations shows that some of them could be traced back to the observation strategy. As pointed out several times, the observation strategy adopted by AIUB to obtain the data used in this study was not intended for the exploitation of the algorithms described in Sec. 2. In particular the requirement of avoiding the singularities described in Sec. 2.3 was not considered, because the very existence of such a problem was not known at the time.

As already discussed, the two algorithms have a limiting time span (different for the two methods) between consecutive tracklets above which a correlation is unlikely to be found. An observation strategy optimized for the use of these algorithms should take into

account this requirement, but for the same reason above, this was not the case for the AIUB data used in this study. The cases in which we were able to attribute the smaller or missed correlations to the observational strategy are highlighted in the tables with the number written between parenthesis: these cases includes both the observations at the same hour in the night and the observations separated by a time interval exceeding 5-6 days.

The cases of 2-tracklet correlations were deemed not reliable. As a matter of fact the typical RMS in the semimajor axis for this orbits were thousands of km for observations taken in the same night. Therefore the probability of being true if a longer time span was available is judged to be very low. A comparison among the 2-tracklet correlations proposed by AIUB and the new method shows a very large fraction of disagreement. Although we would like to confirm this with a specific test, the indication is that 2-tracklet correlations are to be considered as an intermediate data product, not a result, that is they are accepted only if and when it is possible to confirm them with the correlation of a third tracklet.

The results just discussed show a good agreement to the ones obtained by AIUB. The number of cases of "superior" results (columns *larger* and *new*) compensate the "inferior" results (columns *smaller* and *lost*), especially if the cases in which the observing strategy was unsuitable are discounted.

Thus we showed that it is possible to build up a catalog from scratch, without any prior correlation information. This *catalog buildup* phase is necessarily the first phase of a new program such as SSA, because correlation information is not available, or available only for a comparatively small subset of the target population of the new survey.

Moreover, we showed that the presence of non-gravitational perturbations, whose parameters are not known a priori and can be quite large, does not increase the difficulty of the initial catalog buildup. The determination of some non-gravitational perturbation parameters can be done simultaneously with the correlation and orbit determination procedure. To achieve this goal a suitable observing strategy should be used: in particular for the geosynchronous belt one tracklet per night is enough, but "equal hour" singularities and too long time intervals should be avoided.

Of course to obtain the result of building up a large catalog of satellites and space debris, down to sizes smaller than the ones for which orbits are now available, requires the mobilization of appropriate resources. These include sensors more powerful than the current experimental ESASDT (in particular with a larger field of view), and adequate software, such as a scheduler with the capability of taking into account the requirements from orbit determination, and a fully tested correlation and orbit determination software which could be based upon the prototype we have developed.

6 Conclusions

As stated by ESA, "the European Space Situational Awareness (SSA) Programme serves the strategic aims of the European Space Policy (ESP) by supporting the independent capacity to securely, sustainably and safely operate Europe's critical space infrastructure".

In the next few years the SSA initiative will enter its definition and practical implementation phase. One of the goals of the SSA programme is to provide a European catalogue of Earth orbiting objects similar to the American TLE. This goal requires the realization of a Space Surveillance Network of radar and optical sensors able to detect

and track a large number of objects.

Whereas the definition of the network is still in progress, it is clear that the availability of efficient methods for orbit determination is of paramount importance in improving the efficiency of the network. It is worth stressing that an efficient and computationally intensive orbit determination procedure can act in a twofold way in the definition of the network. From one side, given a certain network design, it allows to reach more ambitious goals in terms of cataloguing performances, e.g. allowing the cataloguing of objects with lower diameter limit or the cataloguing of more elusive objects such as the high A/M objects. It must be noted at this stage that the size limit within the TLE catalogue is dictated not only by sensor limitations, but also by limits in the handling and computer processing of the observational data. On the other side, given the preliminary requirements of a surveillance network (e.g., in terms of the minimum size of the objects to be catalogued), the adoption of an efficient orbit determination method allows significant savings in the design of the sensors.

In this paper it was shown how the methods described in Sec. 2 allowed the determination of six-parameters orbits from a standard dataset of optical observations. No a-priori information nor simplified assumptions (such as circular orbits) were required and the observation strategy was completely independent from the design of the methods and not optimized for their use. Even the most demanding cases of high A/M objects were successfully treated.

The results of this study clearly show that the methods described in Sec. 2 can represent an important tool in the SSA data processing. In [1] an extension of the Keplerian integrals method, including the J_2 perturbation, was presented thus allowing the correct treatment of objects in LEO. The application of the method to LEO optical and radar data will be tested in the near future.

Acknowledgments

This study was performed under ESA/ESOC Contract n. 21280/07/D/CS.

References

[1] Farnocchia G.; Tommei G.; Milani A.; Rossi A., 2010, CMDA, 107, 169

[2] Gronchi, G.F., Dimare, L., Milani, A., 2010, CMDA, 107, 299.

[3] Jehn R., S. Ariafar, T. Schildknecht, R. Musci and M. Oswald, 2005, 56^{th} International Astronautical Conference, Fukuoka, Japan, paper IAC-05-B6.1.07.

[4] Liou, J.-C.and Weaver, J. K., 2005, in Danesy Ed., Proceedings of the 4th European Conference on Space Debris, ESA SP-587, Darmstadt, Germany, , 285.

[5] Milani A., Nobili A. and Farinella P.,1987, *Non gravitational perturbations and satellite geodesy*. Adam Hilger Ltd., Bristol and Boston.

[6] Milani, A., 1999, Icarus. 137, 269.

[7] Milani, A., Sansaturio, Chesley, S.R., Icarus. 151, 150.

[8] Milani, A., Gronchi, G.F., de' Michieli Vitturi, M., Knežević, Z., CMDA. 90, 59.

[9] Milani, A., Gronchi, G.F., Knežević, Z., Sansaturio, M.E., Arratia, O., Icarus. 79, 350.

[10] Milani, A., Gronchi, G. F., Farnocchia, D., Tommei, G., Dimare, L., Proc. of the Fifth European Conference on Space Debris. 30 March–2 April 2009, Darmstadt, Germany, SP-672 on CD-Rom.

[11] Milani A.; Gronchi G., 2010, *Theory of orbit determination*, Cambridge University Press

[12] Schildknecht, T., R. Musci, R., Ploner, M., Beutler, G.et al., 2004, Adv. Spa. Res., 34, 901-911 (2004).

[13] Schildknecht, T., Musci, R., Flury, W., Kuusela, J., de Leon, J. and de Fatima Dominguez Palmero, L., 2005, Proceedings of the Fourth European Conference on space debris, Darmstadt, Germany, ESA SP-587, 113.

[14] Schildknecht, T., T. Flohrer, R. Musci, R. Jehn, 2008 Acta Astronautica, 63, 119.

[15] Tommei G.; Milani A.; Rossi A., 2007, CMDA, 97, 289

[16] Tommei, G., Milani, A., Farnocchia, D., Rossi, A.,. Proc. of the Fifth European Conference on Space Debris. 30 March–2 April 2009, Darmstadt, Germany, SP-672 on CD-Rom.

[17] Valk, S., Lemaitre, A., Anselmo, L., 2007, Adv.Spa.Res., 41, 1077